

Journal of Materials Chemistry A

Accepted Manuscript



This is an *Accepted Manuscript*, which has been through the Royal Society of Chemistry peer review process and has been accepted for publication.

Accepted Manuscripts are published online shortly after acceptance, before technical editing, formatting and proof reading. Using this free service, authors can make their results available to the community, in citable form, before we publish the edited article. We will replace this *Accepted Manuscript* with the edited and formatted *Advance Article* as soon as it is available.

You can find more information about *Accepted Manuscripts* in the [Information for Authors](#).

Please note that technical editing may introduce minor changes to the text and/or graphics, which may alter content. The journal's standard [Terms & Conditions](#) and the [Ethical guidelines](#) still apply. In no event shall the Royal Society of Chemistry be held responsible for any errors or omissions in this *Accepted Manuscript* or any consequences arising from the use of any information it contains.



Journal Name

COMMUNICATION

From “Waste to Gold”: One-pot Way to Synthesize Ultrafinely Dispersed Fe₂O₃-based Nanoparticles on N-doped Carbon for Synergistically and Efficiently Water Splitting

Received 00th January 20xx,
Accepted 00th January 20xx

DOI: 10.1039/x0xx00000x

Diefeng Su[†], Jing wang[†], Haiyan Jin, Yutong Gong, Mingming Li, Zhenfeng Pang, Yong Wang*

www.rsc.org/

We report a novel, simple, and one-pot method for the synthesis of ultrafinely dispersed iron oxide based nanoparticles (NPs) embedded in nitrogen doped carbon matrix (denoted as Fe₂O₃/Fe@CN). It is the first time to report that a well-designed iron oxide based hybrid demonstrates high activity and excellent durability for HER in alkaline solution. The catalyst displays a small Tafel slope of 114 mV/decade and good electrocatalytic stability for 30000 seconds. Detailed electrochemical and physical studies indicate that the high HER activity of the hybrid catalyst results from the strong interaction between Fe-based NPs and N-doped graphitic carbon, and especially the synergistic effect of Fe and Fe₂O₃.

The growing demand for energy and the increasing concerns about environment pollution caused by increasing fossil fuels consumption have prompted intensive research interest in seeking sustainable and clean energy.¹ Hydrogen has been considered as a promising alternative for sustainable energy applications because of its high calorific value and environment-friendliness.² And electrocatalytic reduction of water is one of the most effective ways to produce high-purity H₂.^{3, 4} However, developing low-cost and highly efficient electrocatalysts for hydrogen evolution reaction still remains great challenges.

So far, platinum (Pt)-based materials⁵⁻⁷ are the state-of-art HER catalysts, due to unbeatable electrocatalytic HER performance with extremely high exchange current density and small Tafel slope. However, the high price and low abundance of Pt limit their large-scale commercial applications. Therefore, some Pt-like materials, such as molybdenum carbide and molybdenum sulfide⁸⁻¹³ have been

drawing worldwide attention. Additionally, tremendous efforts have been made to explore new HER catalysts based on non-precious transition metals, such as Co, Ni and their molecular derivatives.¹⁴⁻¹⁹ In the past few decades, carbon materials have been widely investigated for energy conversation and storage^{20, 21} owing to their special structure and electronic properties. Very recently, metal-free HER catalysts have been developed and show great potential for electrocatalytic HER. For example, electrocatalysts based on carbon nitride²²⁻²⁴ have been proved that metal-free material is promising for water splitting. Furthermore, a remarkable breakthrough in non-metal electrocatalyst suggested that the dopants of N and P²⁵ were contributed to the enhancement of electrochemical performance for HER applications. It inspires us that we can produce new electrocatalysts, which used to be not suitable for HER, such as non-metal materials, by means of altering their structure and electronic properties. Particularly, we can take advantages of carbon materials²⁶⁻²⁸, which feature unique electronic properties, large specific surface area and well-developed porosity, to modify the structure and electrocatalytic properties of metal-based catalysts.

Currently, Fe is one of the cheapest and abundant metals, and it is expected that artificial Fe-based inorganic compound can act as a cheap HER catalyst. HER catalysts based on iron, such as FeP^{29, 30} and FeS³¹ have recently been widely investigated as hydrogen evolution reaction catalysts and demonstrated comparable activity to the Ni and Co based catalysts. However, the research based on iron oxide for HER is relatively rare. Excitingly, a recent research has been reported that nanoscale Fe₂O₃ supported on N-doped carbon is an effective heterogeneous catalyst for selective hydrogenation of nitroarenes to anilines.³² As hydrogenation and HER both rely on the reversible binding of hydrogen to the catalyst (with hydrogen dissociation and with protons bound to the catalyst to promote hydrogen formation in HER), it is expected that Fe₂O₃ coupled with nitrogen doped carbon may function as HER catalysts.

Herein, we successfully designed a Fe₂O₃-based material embedded in nitrogen doped carbon matrix (denoted as Fe₂O₃/Fe@CN) via simple and efficient thermal condensation of inexpensive starting materials. Electrochemical measurement shows that the catalyst possesses HER overpotential as low as 0.33 V at a current density of 10 mA cm⁻² and good electrocatalytic stability for

Advanced Materials and Catalysis Group, ZJU-NHU United R&D Center, Department of Chemistry, Zhejiang University, Hangzhou 310028, P. R. China.

*Corresponding authors. Tel: (+86)-571-8827-3551, Fax: (+86)-571-8795-1895.

E-mail addresses: chemwy@zju.edu.cn

† These authors contributed equally to this work.

† Electronic supplementary information (ESI) available: Experimental section and characterization results.

30000 seconds in 1M KOH solution, which was comparable to other transformation metal based HER catalysts^{37, 33-35}. To our best knowledge, it is reported for the first time that the well-designed iron oxide based hybrid material has great potential for highly efficient electrocatalytic HER. Detailed electrochemical and physical studies interpret that the high HER activity of the hybrid catalyst results from the strong interaction between Fe-based NPs and N-doped graphitic carbon with large specific surface area, and the synergistic effect of Fe and Fe₂O₃. Notably, the nanohybrid is easily obtained through one-step thermal condensation of low cost starting materials, and the synthetic method is capable of scale-up production for practical applications. The outstanding electrocatalytic performance and low production cost prove that the Fe₂O₃/Fe@CN hybrid material is promising as a desired candidate for non-noble-metal HER catalysts in water splitting. It does not only open up a new perspective for replacing noble metals, but also initiate a new direction for academic research.

Figure 1 illustrates the typical morphology, structure, and composition of the hybrid material Fe₂O₃/Fe@CN, which was calcined at 900 °C in an inert flow. During the material preparation, D-glucosamine hydrochloride, a biomass downstream product, is chosen both as the carbon and nitrogen source; Melamine serves as the soft template³⁶ for the temporary in situ synthesis of carbon nitride. Transmission electron microscope images and scanning transmission electron microscope images (Figure 1a and 1d) show that the metal nanoparticles are well dispersed in carbon matrix, implying well bonding between Fe-based NPs and porous carbon, which would otherwise aggregate³⁷. The average diameter is approximately 15 nm according to the particle size distribution. The HRTEM (Figure 1b & 1c) images demonstrate the presence of both metallic Fe with interplanar

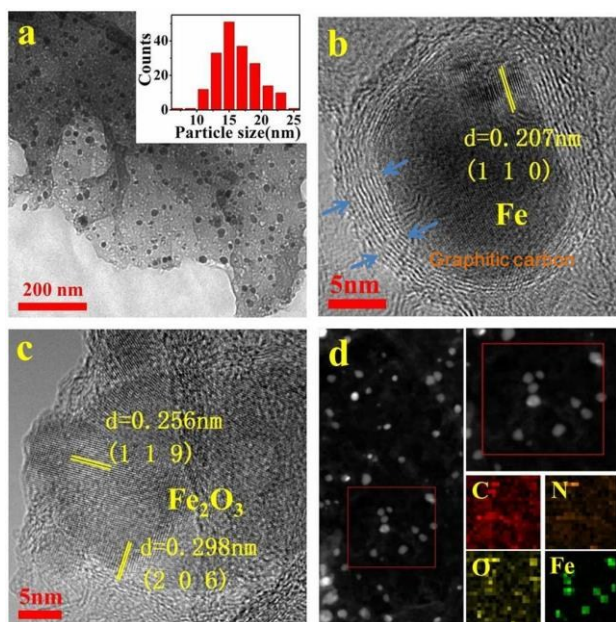


Figure 1. Representative TEM image a, HRTEM images (b, c), STEM image and EDX elemental mapping (d) of Fe₂O₃/Fe@CN. Inset (a) is metal particle size distribution histogram of Fe₂O₃/Fe@CN.

distance of 0.207 nm, and Fe₂O₃ with lattice spacing of 0.256 and 0.298 nm. The X-ray diffraction peaks of Fe₂O₃/Fe@CN (Figure 2a) are consistent with the standard γ -Fe₂O₃ structure (JCPDS No.39-1346)

and cubic Fe (JCPDS No.06-0696), which further confirms the coexistence of the Fe₂O₃ and Fe phases. In addition to XRD analysis, the formation of Fe₂O₃ nanoparticles is further corroborated by XPS measurement (Figure 2b). Apart from apparent peaks at 710.2 and 723.3 eV, a satellite peak at 717.8 eV is recorded from Fe 2p spectrum, verifying the existence of Fe₂O₃ in the hybrid material³⁸. Furthermore, XPS analysis of N1s confirmed that the nitrogen was introduced into the carbon successfully and four kinds of N species, including pyridine N, pyrrole N, quaternary N, and N-oxide could be observed (Figure S1).

It is worth noting that the (0 0 2) peak at 26° attributes to the hexagonal graphite, suggesting that this material has been highly carbonized. Moreover the HRTEM analysis (Figure S2) demonstrates that the graphitic carbon with an interplanar distance of near 0.34 nm further evidence that the hybrid is of well carbonization.³⁹ The graphitic carbon is propitious to improve the matrix electrical conductivity and mechanical stability. This partial graphitization is further affirmed by Raman spectroscopy (Figure 2c). The G band and D band appear around 1590 and 1350 cm⁻¹, corresponding to the first-order scattering of the E_{2g} vibrational mode within aromatic carbon rings and the disorder induced features caused by lattice defects, respectively, unarguably declaring the dual amorphous and crystalline nature of the carbonaceous matrix obtained herein.⁴⁰ Judging from the intensity ratio of D/G band (0.95), it is deduced that the material is indicative of sufficient structural defects⁴¹, possibly resulting in the enhancement of activity in HER.

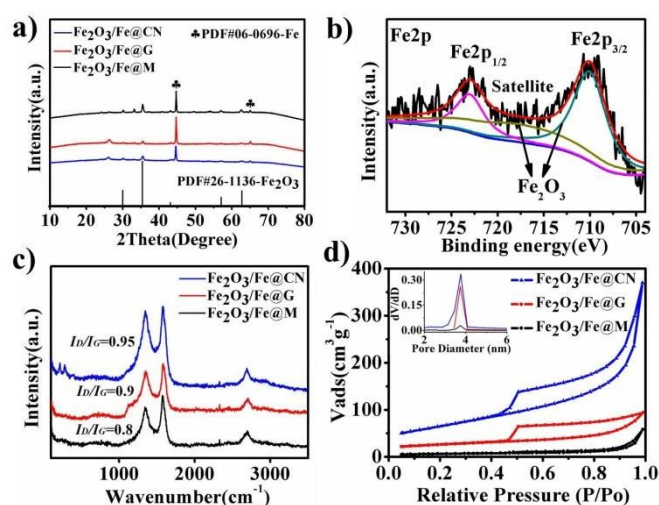


Figure 2. a) XRD patterns, c) Raman spectrum, d) adsorption / desorption isotherms of the Fe₂O₃/Fe@G, Fe₂O₃/Fe@M and Fe₂O₃/Fe@CN, b) XPS Fe2p spectrum of Fe₂O₃/Fe@CN. The inset in d) is the pore size distribution of Fe₂O₃/Fe@CN.

N₂ sorption isotherms were carried out to investigate the textural structure of the hybrid material (Figure 2d). The adsorption isotherm resembles type IV with an obvious capillary condensation occurring at relative pressure 0.4-0.6, affirming the existence of mesopores. By means of analysis on the desorption branch of nitrogen sorption, it was found that the pore diameter clustered together at 3.8 nm, which provided an optimal accessibility for transportation of electrolyte. Moreover, the specific surface areas (Brunauer-Emmett-Teller) were calculated to be 233 m² g⁻¹ (Table S1), providing a plenty of active sites and facilitating the electrolysis of water.

Then we investigated the influence of the carbon resource GAH and soft template melamine on the morphology and structure of the final material. SEM was used to characterize $\text{Fe}_2\text{O}_3/\text{Fe}@M$ and $\text{Fe}_2\text{O}_3/\text{Fe}@G$, which were prepared from the mixture of ferric nitrate & melamine and ferric nitrate & D-glucosamine hydrochloride respectively. The synthetic method was the same as that of $\text{Fe}_2\text{O}_3/\text{Fe}@CN$ (Detailed information, please see the ESI experimental). Our previous report showed that melamine was polymerized to produce graphitic carbon nitride and GAH was condensed to form a carbon skeleton in the interlayer of the carbon nitride during first-stage calcining process at 600 °C. When temperature reached higher than 700 °C, carbon nitride began to decompose and graphene-like N-doped graphitic carbon was formed.³⁶ The SEM images of $\text{Fe}_2\text{O}_3/\text{Fe}@G$ (Figure S3) suggested that many nanoparticles agglomerated together without the soft template of melamine. Agglomeration also existed in the material of $\text{Fe}_2\text{O}_3/\text{Fe}@M$ without the addition of GAH. However, $\text{Fe}_2\text{O}_3/\text{Fe}@CN$ has a flake-like morphology, but some carbon nanotubes were also observed. The special properties of carbon nanotube like good electrical conductivity and special electronic property might contribute to the high HER activity. Additionally, TEM images of the three materials demonstrated that agglomerate phenomena were observed in both of $\text{Fe}_2\text{O}_3/\text{Fe}@M$ and $\text{Fe}_2\text{O}_3/\text{Fe}@G$, but well-dispersed uniform Fe-based NPs emerged in $\text{Fe}_2\text{O}_3/\text{Fe}@CN$ (Figure S4). According to previous reports^{42,43} and above characterizations, doped N would impede the agglomeration of the metal NPs through the interaction between metal atom and nitrogen atom. It was widely accepted that particle size played an important role in heterogeneous catalysis.⁴⁴ Thus, we investigated the N content of the three materials via EA and semiquantitative analysis of XPS (Figure S5). As a result, $\text{Fe}_2\text{O}_3/\text{Fe}@CN$ hybrid showed the highest N content both in bulk and surface phases. Moreover, N_2 sorption isotherms analysis illustrated the specific surface area of $\text{Fe}_2\text{O}_3/\text{Fe}@CN$ was the largest among the three materials. Consequently, the components of GAH and melamine, which served as carbon & nitrogen resource and soft template respectively, were indispensable to produce $\text{Fe}_2\text{O}_3/\text{Fe}@CN$ with ultrafinely dispersed metal NPs, relatively large specific surface area and rich nitrogen content. Similarly, recent research reported that the electrocatalytic activity was influenced by the morphology and specific surface area.⁴⁵ With these surprising findings, it can be predicted that $\text{Fe}_2\text{O}_3/\text{Fe}@CN$ may possess some excellent electrocatalytic performance towards HER.

Thus, we testified the electrocatalytic performance of $\text{Fe}_2\text{O}_3/\text{Fe}@M$, $\text{Fe}_2\text{O}_3/\text{Fe}@G$, and $\text{Fe}_2\text{O}_3/\text{Fe}@CN$, which were deposited with the same loading of approximately 0.28 mg cm⁻² on glassy carbon electrodes (GCEs) in 1M KOH solution using a typical three-electrode setup. As illustrated in linear sweep voltammetry (LSV) curve (Figure 3a), the different materials acted out quite different properties and $\text{Fe}_2\text{O}_3/\text{Fe}@CN$ performed the best, showing the overpotential 0.33 V at a current density of 10 mA cm⁻², comparable to other transition-metal electrocatalysts (Table S2). And the HER activity could be improved by increasing the loading (Figure S6). Figure S7 displayed an optical photograph of the hybrid catalysts on the GCE during LSV scan, revealing the production of many hydrogen bubbles on the electrode surface. Tafel plots were shown in Figure 3b, which were fit to the Tafel equation ($\eta = b \cdot \log j + a$, where j is the current density and b is the Tafel slope), yielding Tafel slopes of approximately 128, 142, and

114 mV/dec for $\text{Fe}_2\text{O}_3/\text{Fe}@M$, $\text{Fe}_2\text{O}_3/\text{Fe}@G$, and $\text{Fe}_2\text{O}_3/\text{Fe}@CN$, respectively. By extrapolation from Tafel equation, the exchange current density j_0 of $\text{Fe}_2\text{O}_3/\text{Fe}@CN$ was calculated to be 12.2 $\mu\text{A cm}^{-2}$, which was close to the reported transition metal catalysts for HER in alkaline solution^{46,47}. These Tafel slopes for all the catalysts revealed that the HER procedure was controlled by Volmer reaction step.⁴⁸ Electrochemical impedance spectroscopy (EIS) was further applied to illustrate the relative enhancement of the catalytic activity for $\text{Fe}_2\text{O}_3/\text{Fe}@CN$. The Nyquist plots of the EIS response (Figure 3c) indicated the charge transfer resistance of $\text{Fe}_2\text{O}_3/\text{Fe}@CN$ is the smallest. According to Tafel and EIS measurement, the $\text{Fe}_2\text{O}_3/\text{Fe}@CN$ displayed the best kinetic performance.

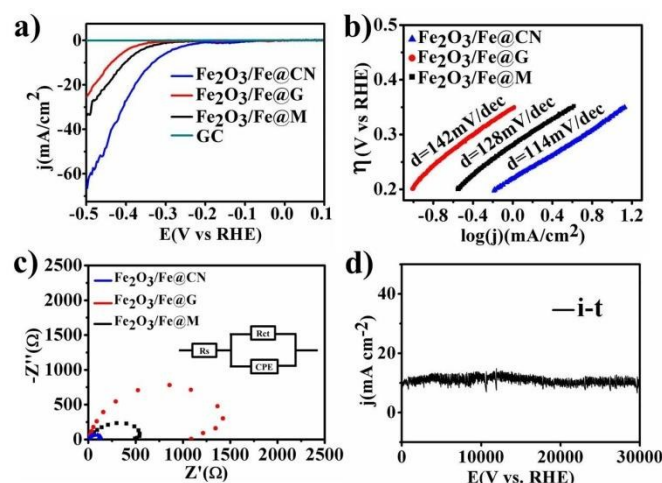


Figure 3. a) Linear sweep voltammetry, b) Tafel plots, c) Nyquist plots of $\text{Fe}_2\text{O}_3/\text{Fe}@G$, $\text{Fe}_2\text{O}_3/\text{Fe}@M$ and $\text{Fe}_2\text{O}_3/\text{Fe}@CN$ under the loading of 0.28 mg cm⁻² in 1M KOH, d) Time dependence of the current density of $\text{Fe}_2\text{O}_3/\text{Fe}@CN$ at $\eta = 0.35$ V under the loading of 0.28 mg cm⁻² in 1M KOH

For commercial applications, electrocatalysts were required to have high stability. To assess the stability of $\text{Fe}_2\text{O}_3/\text{Fe}@CN$ in HER, the time dependence of the current density was executed under basic solution. Figure 3d prompted the material maintained its electrocatalytic activity, giving a constant current density of ca. 10 mA cm⁻² for 30000 seconds. The result implied $\text{Fe}_2\text{O}_3/\text{Fe}@CN$ with great durability. TEM images of the used sample revealed that the morphology and nanoparticle size remained almost unchanged after electrochemical tests (Figure S8).

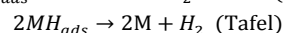
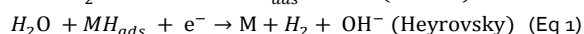
To figure out the reason of different HER activity among the aforementioned three materials, XRD characterization was firstly applied, which disclosed the same Fe-based component and did not make a distinction among the various three catalysts (Figure 2a). Consequently, it is deduced that the carbon support may play the key role in the HER catalysis. According to the above characterizations on the three materials, the high activity of $\text{Fe}_2\text{O}_3/\text{Fe}@CN$ might be ascribed to large specific surface area and rich nitrogen content, which was in agreement with previous reports.⁴⁹ Large specific surface area is expected to exhibit the high exposure of effective active sites, which are responsible for the excellent HER activity.⁵⁰ Besides, electrochemical double layer capacitances (C_{dl}) are considered as a describer to evaluate the effective surface area. Figure S9 clearly showed that $\text{Fe}_2\text{O}_3/\text{Fe}@CN$ displayed the biggest C_{dl} of 16.2 mF/cm², leading to the best performance among the three materials. On the

other hand, the doping of nitrogen does not only prevent metal NPs from aggregating, but also may act as active site for HER catalysis.²² To further understand the effect of N, another controlled experiment was carried out on the HER activity of Fe₂O₃/Fe@GL, manifesting the activity was inferior to Fe₂O₃/Fe@CN. It made no significant difference between Fe₂O₃/Fe@CN and Fe₂O₃/Fe@GL in morphology and structure, but the nitrogen content of Fe₂O₃/Fe@GL was lower than that of Fe₂O₃/Fe@CN, which might be a possible reason of relatively lower HER activity (Figure S10). Additionally, the *I_d/I_g* of Fe₂O₃/Fe@CN (Figure 2c) was the biggest, implying plenty of defective sites³², which might be supposed as one possible reason for the increasing HER performance. Consequently, the as-prepared Fe₂O₃/Fe@CN via one-pot method with large specific surface area and rich N content might be a promising HER catalysts for practical applications.

Interestingly, it was found that the interaction between iron oxide based NPs and carbon support might play an important role on the enhancement of Fe₂O₃/Fe@CN catalyst for HER. To further shed light on our hypothesis, we examined the Fe₂O₃, ph-Fe₂O₃/AC, Fe₂O₃/AC with the same loading of 0.28 mg cm⁻² in 1M KOH solution (ph-Fe₂O₃/AC was a mechanical mixture of commercial nanoscale Fe₂O₃ and activated carbon; Fe₂O₃/AC was a composite of Fe₂O₃ and carbon, prepared according to report⁵¹). From LSV curve (Figure 4a), it was easy to reach an agreement that the activity of Fe₂O₃ could be significantly advanced by introducing carbon carrier. Furthermore, by comparison of ph-Fe₂O₃/AC and Fe₂O₃/AC, it was reconfirmed that the stronger interaction between the metal NPs and support, the better performance of HER. In order to understand the interaction between Fe₂O₃ and carbon matrix, FT-IR analysis, Raman spectrum and XPS were utilized. Compared with the pure Fe₂O₃ from FT-IR analysis, the blue-shift absorption of Fe₂O₃/Fe@CN around 640 cm⁻¹ confirmed the formation of C-O-Fe (Figure 4b).^{54, 52} Similarly in Raman spectra (Figure S11), peaks for Fe₂O₃/Fe@CN were detected with Raman shift, possibly stemming from the interaction between Fe₂O₃ and carbon support. In addition, the high-resolution of O1s XPS spectrum for the

Fe₂O₃/Fe@CN (Figure S12) material suggested the existence of C-O-Fe bond which indicated a possible interaction between the Fe-based NPs and carbon matrices.⁵³

Further, it was protocolled that the Fe₂O₃ and Fe might be synergistically active sites for HER catalysis. To verify this assumption, we tried to separate the two components. TEM images clearly indicated that most of the metallic Fe was covered with graphitic carbon. Thus the material was washed with 2M HNO₃ solution and the obtained product was named as AT-Fe₂O₃/Fe@CN. From XRD analysis (Figure 4c), it could be found that the phase of Fe₂O₃ was removed and the metallic Fe was reserved due to the protection from outside graphitic carbon. The existence of metallic Fe was verified by the HRTEM image of AT-Fe₂O₃/Fe@CN as well (Figure S13). Meanwhile, the absence of characteristic signal for metallic Fe in the high-resolution of Fe2p XPS spectrum for Fe₂O₃/Fe@CN and the ignorable Fe2p signal in XPS spectrum for AT-Fe₂O₃/Fe@CN further demonstrated that the metallic Fe was embedded in the graphitic carbon (Figure S14). Thus it could be supposed that the phase of metallic Fe in Fe₂O₃/Fe@CN was reserved after acid treatment. Then the electrocatalytic performance of the two materials under the same condition was compared (Figure 4d). As a result, AT-Fe₂O₃/Fe@CN showed inferior activity, revealing the synergistic effects of Fe₂O₃ and Fe on HER catalysis. Moreover, the performance of AT-Fe₂O₃/Fe@CN still could not exceed that of Fe₂O₃/Fe@CN even increasing the loading (Figure 4d, S15), which further highlighted the synergistic effects. To better understand the synergistic effects, it was essential to investigate whether the ratio of the two components affected the HER activity. Thus we synthesized the materials under the same method as Fe₂O₃/Fe@CN except for the different calcination temperature. It was found that the materials with different ratio of Fe/Fe₂O₃ exhibited similar catalytic performance, which meant that the ratio did not have a strong relation with the HER activity to some extent (Figure S16). In alkaline media, the HER pathway could be via the Volmer–Heyrovsky process or Volmer–Tafel pathways.^{54, 55} (Eq 1)



Here, the Fe₂O₃ site preferentially adsorbed OH⁻ generated by water decomposition thanks to the strong electrostatic affinity to the locally positively charged Fe₂p species and more unfilled d orbitals in Fe₂p than Fe metal, while a nearby Fe site would facilitate H adsorption, imparting synergistic HER catalytic activity to Fe₂O₃/Fe@CN. Admittedly, detailed mechanistic insights into electrocatalysis of the Fe₂O₃/Fe@CN hybrid material remains to be further confirmed.

Conclusions

In summary, we successfully designed a Fe₂O₃/Fe@CN hybrid material through one-pot method as an efficient HER catalyst. The nitrogen doped carbon matrix provides reasonable pore structure and helps to disperse Fe-based nanoparticles, which facilitates the HER process. The interaction between active sites and support also plays a key role in improving electronic performance for HER. Additionally, the enhancement of activity on HER catalysis is ascribed to synergistic effects of Fe₂O₃ and Fe. The highly active Fe₂O₃/Fe@CN

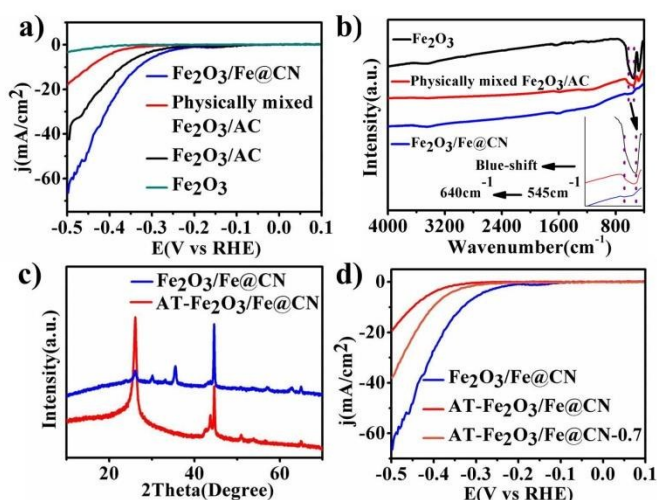


Figure 4. a, d) Linear sweep voltammetry of Fe₂O₃/Fe@CN, Fe₂O₃, ph-Fe₂O₃/AC, Fe₂O₃/AC, AT-Fe₂O₃/Fe@CN, under the loading of 0.28 mg cm⁻² and AT-Fe₂O₃/Fe@CN-0.7 under the loading of 0.7 mg cm⁻² in 1M KOH, b) FT-IR patterns of Fe₂O₃/Fe@CN, Fe₂O₃ and ph-Fe₂O₃/AC, c) XRD patterns of AT-Fe₂O₃/Fe@CN and Fe₂O₃/Fe@CN.

electrocatalyst with low cost, earth abundance and environmental friendliness is promising for future water-splitting devices. Moreover, it does not only open up a new perspective for replacing noble metals, but also initiate a new direction for academic research.

Acknowledgments

Financial support from the National Natural Science Foundation of China (21376208 & J1210042), the Zhejiang Provincial Natural Science Foundation for Distinguished Young Scholars of China (LR13B030001), the Specialized Research Fund for the Doctoral Program of Higher Education (J20130060), the Program for Zhejiang Leading Team of S&T Innovation, the Fundamental Research Funds for the Central Universities, and the Partner Group Program of the Zhejiang University and the Max-Planck Society are greatly appreciated.

Notes and references

- M. S. Dresselhaus and I. L. Thomas, *Nature*, 2001, **414**, 332-337.
- M. G. Walter, E. L. Warren, J. R. McKone, S. W. Boettcher, Q. Mi, E. A. Santori and N. S. Lewis, *Chem. Rev.*, 2010, **110**, 6446-6473.
- J. D. Holladay, J. Hu, D. L. King and Y. Wang, *Catal. Today*, 2009, **139**, 244-260.
- K. Zeng and D. K. Zhang, *Prog. Energy Combust. Sci.*, 2010, **36**, 307-326.
- S. Schuldiner, *J. Electrochem. Soc.*, 1952, **99**, 488-494.
- W. Sheng, H. A. Gasteiger and Y. Shao-Horn, *J. Electrochem. Soc.*, 2010, **157**, B1529-B1536.
- H. Hu, Z. Jiao, J. Ye, G. Lu and Y. Bi, *Nano Energy*, 2014, **8**, 103-109.
- Y.-H. Chang, C.-T. Lin, T.-Y. Chen, C.-L. Hsu, Y.-H. Lee, W. Zhang, K.-H. Wei and L.-J. Li, *Adv. Mater.*, 2013, **25**, 756-760.
- D. J. Li, U. N. Maiti, J. Lim, D. S. Choi, W. J. Lee, Y. Oh, G. Y. Lee and S. O. Kim, *Nano Lett.*, 2014, **14**, 1228-1233.
- Y. Li, H. Wang, L. Xie, Y. Liang, G. Hong and H. Dai, *J. Am. Chem. Soc.*, 2011, **133**, 7296-7299.
- L. Liao, S. Wang, J. Xiao, X. Bian, Y. Zhang, M. D. Scanlon, X. Hu, Y. Tang, B. Liu and H. H. Girault, *Energy Environ. Sci.*, 2014, **7**, 387-392.
- S. Chen, J. Duan, Y. Tang, B. Jin and S. Zhang Qiao, *Nano Energy*, 2015, **11**, 11-18.
- L. Zhang, H. B. Wu, Y. Yan, X. Wang and X. W. Lou, *Energy Environ. Sci.*, 2014, **7**, 3302-3306.
- M. A. McArthur, L. Jorge, S. Coulombe and S. Omanovic, *J. Power Sources*, 2014, **266**, 365-373.
- B. Pierozynski, T. Mikołajczyk and I. M. Kowalski, *J. Power Sources*, 2014, **271**, 231-238.
- S. Baranton and C. Coutanceau, *Appl. Catal. B: Environ.*, 2013, **136-137**, 1-8.
- X. Zou, X. Huang, A. Goswami, R. Silva, B. R. Sathe, E. Mikmekov \acute{a} and T. Asefa, *Angew. Chem. Int. Ed.*, 2014, **53**, 4372-4376.
- M. Gong, W. Zhou, M.-C. Tsai, J. Zhou, M. Guan, M.-C. Lin, B. Zhang, Y. Hu, D.-Y. Wang, J. Yang, S. J. Pennycook, B.-J. Hwang and H. Dai, *Nat. Commun.*, 2014, **5**.
- H. Jin, J. Wang, D. Su, Z. Wei, Z. Pang and Y. Wang, *J. Am. Chem. Soc.*, 2015, **137**, 2688-2694.
- A. D. Roberts, X. Li and H. Zhang, *Chem. Soc. Rev.*, 2014, **43**, 4341-4356.
- Y. Zhou, S. L. Candelaria, Q. Liu, Y. Huang, E. Uchaker and G. Cao, *J. Mater. Chem. A*, 2014, **2**, 8472-8482.
- Y. Zheng, Y. Jiao, Y. Zhu, L. H. Li, Y. Han, Y. Chen, A. Du, M. Jaroniec and S. Z. Qiao, *Nat. Commun.*, 2014, **5**.
- M. Shalom, S. Gimenez, F. Schipper, I. Herraiz-Cardona, J. Bisquert and M. Angew. Chem. Int. Ed., 2014, **53**, 3654-3658.
- Y. Zhao, F. Zhao, X. Wang, C. Xu, Z. Zhang, G. Shi and L. Qu, *Angew. Chem. Int. Ed.*, 2014, 13934-13939.
- Y. Zheng, Y. Jiao, L. H. Li, T. Xing, Y. Chen, M. Jaroniec and S. Z. Qiao, *ACS Nano*, 2014, **8**, 5290-5296.
- Y. Gong, Z. Wei, J. Wang, P. Zhang, H. Li and Y. Wang, *Sci. Rep.*, 2014, **4**.
- C. Han, J. Wang, Y. Gong, X. Xu, H. Li and Y. Wang, *J. Mater. Chem. A*, 2014, **2**, 605-609.
- B. Xia, Y. Yan, X. Wang and X. W. Lou, *Mater. Horiz.*, 2014, **1**, 379-399.
- Y. Xu, R. Wu, J. Zhang, Y. Shi and B. Zhang, *Chem. Commun.*, 2013, **49**, 6656-6658.
- P. Jiang, Q. Liu, Y. Liang, J. Tian, A. M. Asiri and X. Sun, *Angew. Chem. Int. Ed.*, 2014, **53**, 12855-12859.
- C. Di Giovanni, W.-A. Wang, S. Nowak, J.-M. Grenèche, H. Lecoq, L. Mouton, M. Giraud and C. Tard, *ACS Catal.*, 2014, **4**, 681-687.
- R. V. Jagadeesh, A.-E. Surkus, H. Junge, M.-M. Pohl, J. Radnik, J. Rabeah, H. Huan, V. Schünemann, A. Brückner and M. Beller, *Science*, 2013, **342**, 1073-1076.
- J. Kibsgaard, Z. Chen, B. N. Reinecke and T. F. Jaramillo, *Nat. Mater.*, 2012, **11**, 963-969.
- J. Deng, P. Ren, D. Deng, L. Yu, F. Yang and X. Bao, *Energy Environ. Sci.*, 2014, **7**, 1919-1923.
- Z. Chen, D. Cummins, B. N. Reinecke, E. Clark, M. K. Sunkara and T. F. Jaramillo, *Nano Lett.*, 2011, **11**, 4168-4175.
- J. Wang, Z. Xu, Y. Gong, C. Han, H. Li and Y. Wang, *ChemCatChem*, 2014, **6**, 1204-1209.
- J. Ma, L. T. B. La, I. Zaman, Q. Meng, L. Luong, D. Ogilvie and H.-C. Kuan, *Macromol. Mater. Eng.*, 2011, **296**, 465-474.
- T. Fujii, F. M. F. de Groot, G. A. Sawatzky, F. C. Voogt, T. Hibma and K. Okada, *Phys. Rev. B*, 1999, **59**, 3195-3202.
- E. D. Grayfer, A. S. Nazarov, V. G. Makotchenko, S.-J. Kim and V. E. Fedorov, *J. Mater. Chem.*, 2011, **21**, 3410-3414.
- V. Chandra, J. Park, Y. Chun, J. W. Lee, I.-C. Hwang and K. S. Kim, *ACS Nano*, 2010, **4**, 3979-3986.
- A. Nsabimana, X. Bo, Y. Zhang, M. Li, C. Han and L. Guo, *J. Colloid Interface Sci.*, 2014, **428**, 133-140.
- Y. Wang, J. Yao, H. Li, D. Su and M. Antonietti, *J. Am. Chem. Soc.*, 2011, **133**, 2362-2365.
- X. Xu, Y. Li, Y. Gong, P. Zhang, H. Li and Y. Wang, *J. Am. Chem. Soc.*, 2012, **134**, 16987-16990.
- R. J. White, R. Luque, V. L. Budarin, J. H. Clark and D. J. Macquarrie, *Chem. Soc. Rev.*, 2009, **38**, 481-494.
- L. Liao, J. Zhu, X. Bian, L. Zhu, M. D. Scanlon, H. H. Girault and B. Liu, *Adv. Funct. Mater.*, 2013, **23**, 5326-5333.
- B. Liu, J.-B. He, Y.-J. Chen, Y. Wang and N. Deng, *Int. J. Hydrogen Energy*, 2013, **38**, 3130-3136.
- D. M. F. Santos, L. Amaral, B. Šljukić, D. Macciò, A. Saccone and C. A. C. Sequeira, *J. Electrochem. Soc.*, 2014, **161**, F386-F390.
- F. Rosalbino, D. Macciò, A. Saccone and G. Scavino, *Int. J. Hydrogen Energy*, 2014, **39**, 12448-12456.

COMMUNICATION

Journal Name

49. A. B. Fuertes, G. A. Ferrero and M. Sevilla, *J. Mater. Chem. A*, 2014, **2**, 14439-14448.
50. M. A. Lukowski, A. S. Daniel, F. Meng, A. Forticaux, L. Li and S. Jin, *J. Am. Chem. Soc.*, 2013, **135**, 10274-10277.
51. Y. Li, C. Zhu, T. Lu, Z. Guo, D. Zhang, J. Ma and S. Zhu, *Carbon*, 2013, **52**, 565-573.
52. S. Hu, K. M. Vogel and T. G. Spiro, *J. Am. Chem. Soc.*, 1994, **116**, 11187-11188.
53. J. Zhou, H. Song, L. Ma and X. Chen, *RSC Advances*, 2011, **1**, 782-791.
54. J. O. M. Bockris and E. C. Potter, *J. Electrochem. Soc.*, 1952, **99**, 169-186.
55. J. G. N. Thomas, *Transactions of the Faraday Society*, 1961, **57**, 1603-1611.